Self-sensing concrete repairs based on alkali-activated materials: recent progress

Marcus Perry
Dept. of Civil & Environmental Engineering
University of Strathclyde
Glasgow, UK
m.perry@strath.ac.uk

Lorena Biondi
Dept. of Civil & Environmental Engineering
University of Strathclyde
Glasgow, UK

Jack McAlorum
Dept. of Civil & Environmental Engineering
University of Strathclyde
Glasgow, UK

Christos Vlachakis
Dept. of Civil & Environmental Engineering
University of Strathclyde
Glasgow, UK

***Abstract*—This paper provides an overview of recent highlights from our development of robotically deployed, self-sensing alkali-activated materials: a cement technology which can be used to simultaneously repair and monitor concrete structures. While strain and temperature sensing using these materials has already been demonstrated, this paper focuses on recent developments in robotic spray coating and 3D printing, and in moisture, chloride, and damage monitoring, showing pilot data. The electrical impedance of self-sensing materials follows an exponential decrease with increasing levels of moisture, chloride contamination and temperature as expected. The work demonstrates the promise of using these novel self-sensing materials for measuring environmental measurands that are responsible for the majority of concrete structural health degradation in the field.**

***Index Terms*—component, formatting, style, styling, insert**

I. Introduction

Degradation of reinforced concrete costs the global economy an estimated $300–400 bn per year [1], [2]. Asset managers in developed nations are struggling to keep on top of concrete maintenance, and as a result, our infrastructure faces an increasing threat to its resilience despite being overdesigned [3]–[6].

We know that this challenge can be better met with optimised, pro-active maintenance, and improved structural design [7], but all of this demands real-time structural data. Sensors for locating and quantifying salt water (chloride) contamination, cracking, moisture and strain in concrete are therefore of keen interest to the civil structural health monitoring community. This includes industrialists in the nuclear, transport, and off-shore energy generation sectors, as these industries have significant inventories of high-value, safety-critical coastal and marine concrete assets.

In this paper, we outline our recent progress in the development of robotically deployable, self-sensing repair materials for concrete, providing an overview of recent work, and glimpses of pilot data. Our self-sensing repairs are based on Alkali Activated Materials (AAMs) — a class of cementitious binders with diverse and tuneable material properties [8]. Once cured, AAMs exhibit similar thermal and mechanical properties to ordinary Portland cement and adhere strongly to concrete substrates. They are chemically stable and have electrical conductivities in the range 10^{-6} S/cm to 10^{-3} S/cm depending on mix design [9], [10]. These properties make AAMs highly suited to concrete monitoring and maintenance applications: they have already been developed as sensors for strain and temperature [11]–[15] and as concrete repair materials [15]–[17].

Numerous methods for continuous moisture, chloride, strain and damage monitoring in concrete have already been proposed, including: fibre-optic sensors [18], [19]; concrete electrical impedance measurements [20]–[31]; dielectric permittivity and capactive sensors [32]–[36]; and NEMS/MEMS (nano-/micro- electro-mechanical systems) sensors [37]. We will not criticize these other approaches for their cost or performance — each can be viable in the face of a specific application. What will do is state that the AAM sensors discussed in this paper offer two unique benefits: i) they are multi-functional, offering both sensing and repair capability; and ii) they can be applied as 2-dimensional repair, or used as a 3-dimensional concrete composite, and so could support truly distributed sensing with further development [38]. Before distributed sensing can be developed further, we must first demonstrate that point sensing using AAMs is feasible — this is the purpose of the work presented in this paper.

II. Theory and background

A. Alkali-activated materials: a brief introduction

Alkali-activated materials (AAMs) are cementitious binders with diverse and tuneable material properties [8]. They are synthetized by adding an alkaline solution, called an activator,

Some parts of the works described here were funded by the Advanced Nuclear Research Centre (ANRC-27), the National Nuclear Laboratory ICASE award (NNL/UA/022), EPSRC (EP/L014041/1), the Royal Society (RG160748) and the Scottish Funding Council's Oil & Gas Technology Centre.

This is a peer reviewed, accepted author manuscript of the following research article: Perry, M., Biondi, L., McAlorum, J., & Vlachakis, C. (2021). Self-sensing concrete repairs based on alkali-activated materials: recent progress. In 2021 IEEE International Instrumentation and Measurement Technology Conference (I2MTC) [9459969] (Conference Record - IEEE Instrumentation and Measurement Technology Conference; Vol. 2021-May). IEEE. https://doi.org/10.1109/I2MTC50364.2021.945996

(often comprised of sodium hydroxide, NaOH, and sodium silicate, Na_2SiO_3) to raw materials which are rich in aluminium and silicon. Examples of such raw materials include:

- **Fly ash**, a byproduct of coal combustion. Fly ash AAMs exhibit a high workability when uncured, and a high durability and strength, and a low shrinkage once cured [39], [40]. While fly ash is still a plentiful waste resource, its global supply chain now faces uncertainty as coal plants are decomissioned in favour of greener energy sources.
- **Metakaolin**, produced by calcining kaolin (china clay) at elevated temperatures of 200–300 °C. Metakaolin AAMs tend to be more viscous, and can exhibit a greater propensity to undergo shrinkage, and hence delamination and cracking. Shrinkage is often controlled by adding plastic fibres to the mix.

Regardless of the precursor choice, AAM binders can be used as an alternative to ordinary Portland cement, acting as a repair material for existing concrete structures, or being mixed with aggregates to produce construction materials in the form of an AAM concrete.

B. Ionic conductivity

AAMs exhibit a higher electrical conductivity than ordinary Portland cements. This stems from the alkali metal ions (in our case Na^+) introduced by the activator solution [9], [17]. A proportion of the population of these ions is actively bonded to the negatively charged alumino-silicate matrix. The remaining mobile ions increase the ionic content of the water inside the cured material's pores, migrating along the pore network and acting as carriers of electrical current under an applied voltage [10], [41].

For this reason, AAMs have been referred to as solid electrolytes, electrolytic conductors, or ionic conductors. Measured changes in the electrical conductivity of AAMs under imposed loading conditions allow these materials to be employed as sensors [11]–[14].

C. Electrochemical impedance spectroscopy (EIS)

AAMs can be electrically interrogated using metal electrodes, which are embedded prior to curing, or affixed with electrically conductive epoxies post-curing. This produces an AAM sensor cell, as illustrated in Figure 1.

Standard circuits are comprised of electronic conductors, but AAM sensors are a composite of electronic conductors (the metal electrodes) in contact with an ionic conductor (the AAM). They are therefore classed as an electrochemical system, and exhibit behaviors that are not present in most standard electronic sensors.

Electrochemical Impedance Spectroscopy (EIS) is a non-destructive technique that can be used to analyze electrochemical systems, like AAM sensors, both at rest and in response to external measurands. In potentiostatic EIS, the frequency-dependent current response of the sensor cell, $I(t)$, is measured during an applied, time-varying voltage excitation, $V(t)$:

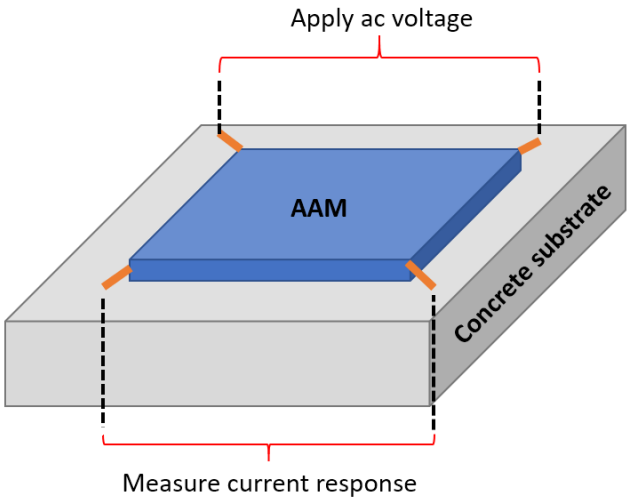

Fig. 1. Diagram showing how the impedance of an AAM patch can be interrogated using a four electrode configuration.

$$\begin{aligned} V(t) &= V_0 cos(\omega t), \\ I(t) &= I_0 cos(\omega t - \phi(\omega)). \end{aligned} \tag{1}$$

Here, V_0 and I_0 are the amplitudes of the applied voltage and measured current respectively, $\phi(\omega)$ is the frequency-dependent phase difference between $V(t)$ and $I(t)$, and $\omega = 2\pi f$ is the radial frequency of applied ac voltage. The electrical impedance of the cell, $\boldsymbol{Z}$, can be defined using Euler notation as [42]:

$$\boldsymbol{Z} = \frac{V(t)}{I(t)} = Z_{mod}(cos(\phi) + isin(\phi)) = Z_{mod}e^{i\phi}, \tag{2}$$

where i is the imaginary unit, $Z_{mod}(\omega) = |Z|$ is the frequency-dependent magnitude or modulus of the impedance, and $\phi = \arg(Z)$ is the phase angle between real and imaginary components.

The real component of the impedance, $Z_{real} = Re(Z)$, is the electrical resistance of the cell, while the imaginary component, $Z_{imag} = Im(Z)$, is its reactance. Inductive elements in a sensor cell, L, cause current changes to lag behind voltage, as $Z_{imag} = i\omega L$. Capacitive elements, C, meanwhile, cause current changes to lead the voltage as $Z_{imag} = -\frac{i}{\omega C}$. Acquired EIS impedance data are typically assessed using a combination of Bode plots (plots of Z_{mod} and ϕ against swept frequency), and Nyquist plots (plots of Z_{real} against Z_{imag}). Figure 2 shows a typical Bode plot for an AAM sensor, demonstrating its predominantly capactive behaviour (phase angles are generally negative).

D. Sensing principle

Bulk electrical conductivity in cementitious materials is a function of the conductivity of the pore solution, σ_0, the

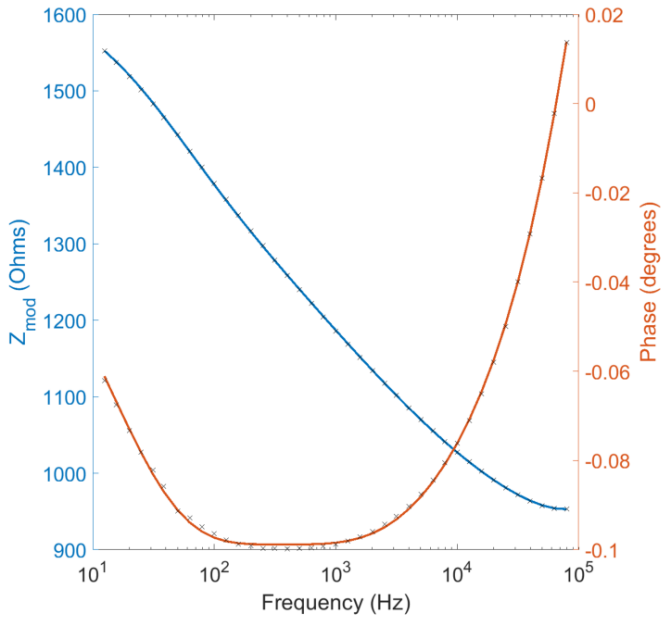

Fig. 2. A typical Bode plot for an AAM sensor, showing phase and impedance modulus response at frequencies between 10 Hz and 100 kHz.

volume of the pore network filled with pore solution, ϕ_{con}, and the connectivity factor of the pore network, β [30]:

$$\sigma = \sigma_0 \phi_{con} \beta. \tag{3}$$

It is currently believed that AAMs follow this same principle, so that their conductivities, σ, depend on measurands which alter the three terms on the right hand side of equation (3).

Examples of measurands which are known to affect AAM conductivity (and hence electrical impedance) include:

- **Temperature**: Increasing the temperature of an AAM enhances ion mobility and encourages electrolytic dissociation, both of which increase σ_0. Provided there is no evaporation of water at elevated temperatures, AAM conductivity, σ, increases exponentially with temperature, T [43].
- **Moisture**: Water content within an AAM can affect all three terms in equation (3). It reduces the conductivity of the pore solution, σ_0, by diluting it, but meanwhile increases pore fill volume, ϕ_{con}, and connectivity, β [28]. At very low water contents, conductivity can decrease dramatically as the liquid electrolyte cannot cover the internal surfaces of the pores [28]. Electrical conductivity increases exponentially with internal water content [22].
- **Strain and cracking**: Strain and cracking affect the geometry and connectivity within AAM samples. Cracking of the sample can lead to very obvious step-changes in impedance. The stress-strain response of an AAM is similar to the underlying concrete substrate: it is linear for low strains, but then becomes non non-linear as strains increase. Electrical conductivity change is proportional to strain for low levels of strain.
- **Ionic contamination**: Exposure of an AAM to sodium chloride (e.g. via sea water or de-icing salts) can affect the ionic balance within the material, and so the density of charge carriers. In general, increases in ionic concentration improve electrical conductivity up until a point: oversaturation can reduce ion mobility, reducing the conductivity gains.

All of these measurands are useful to measure in a concrete monitoring and maintenance context: all can be linked to concrete degradation mechanisms or indicators of performance. Strain and temperature have been reported on in plenty of previous studies. Here, we focus on new developments in moisture, chloride contamination, and damage sensing.

A general equation for the AAM sensor's response to moisture, temperature and ionic concentration, has the following form:

$$ln\left(\frac{Z_{mod}}{Z_{mod,0}}\right) = \frac{G_1}{T} + G_2 T + \frac{G_3}{W} + G_4 c, \tag{4}$$

where $G_{1,\ldots,4}$ are constants, T is the temperature, W is the internal water content, and c is the internal ionic concentration. There may, following characterisation, be cross-dependencies found between measurands at extreme values. As with any sensor, decoupling these measurands typically requires reference sensors, or reference AAM patches.

III. Methods

Mix designs for AAMs widely, and some examples of both fly-ash and metakolin mixes may be found in our previous work. This paper will instead focus on our recent progress in AAM sensing, and the deployment of those sensors.

A. Deployment

AAMs can be deployed manually via spray-coating, trowelling, or painting concrete surfaces. However, in a construction context, it is a lack of thought around the *deployment* of monitoring technologies which is causing them to be less widely utilised. This is because manual deployment:

- **Bears a high cost**: Sensors themselves are often affordable, but their installation campaigns can pose significant labour costs, risks to productivity, and risks to personnel.
- **Deliver uncertain returns**: All sensors face performance loss when installation is done incorrectly — sensor repeatability and robustness in the field are less about what is written on a datasheet, and more about the quality workmanship during installation [44]. This is a problem: humans frequently make mistakes [45] and then forget them [46]. This has a pronounced impact on our confidence in using sensor data to make design and maintenance decisions, and could harm industry's image of otherwise promising technologies [47], [48].

To solve this, our group have been looking at robotic deployment methods for AAM, including 3D printing and robotic spray coating. The concept is illustrated in Figure 3. Mounting a spray coater or extrusion nozzle to the tool-end of a six-axis

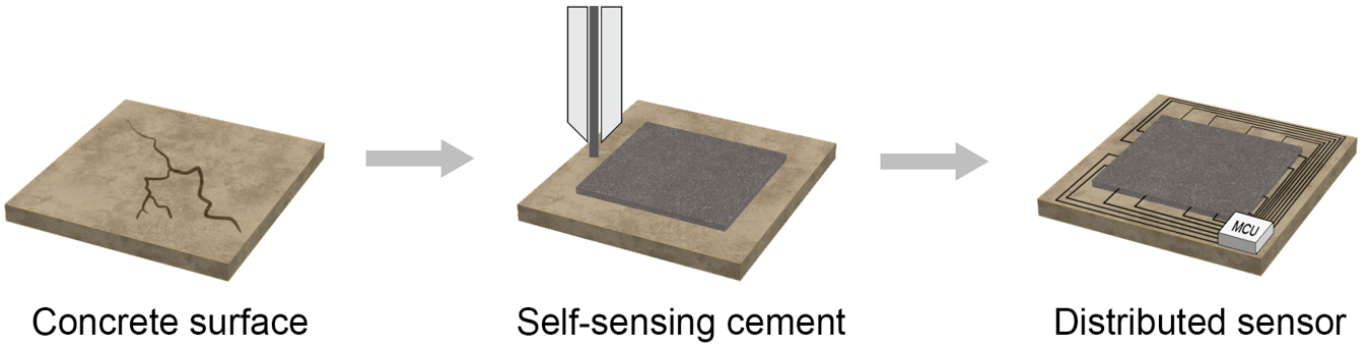

Fig. 3. A concept drawing of the robotic deployment of AAM sensor patches onto damaged concrete surfaces.

robot or a mobile gantry could ensure precise, repeatable and remote deposition of AAM sensors onto concrete substrates in the field or in precast manufacturing plants. This will tackle some of the barriers to sensor deployment in construction, and we hope, improve the repeatability of the sensing from patch to patch.

In both cases, AAM is fed into a progressive cavity extruder from a dispenser fit with air supply pressure of 1 bar. This ensures material flow into the screw cavity regardless of extruder orientation. The AAM is either extruded onto the surface of the concrete substrate directly (when 3D printing) or atomised post-extrusion (when spray coating).

B. Interrogation

In our work, electrodes are usually placed onto concrete substrates prior to AAM patch deployment. The curing AAM then binds to the electrodes and substrate.

Potentiostatic EIS is used to interrogate patches. A 10 mV voltage is applied to the AAM cells. The low magnitude of the voltage produces a pseudo-linear current response, allowing impedance to be calculated more conveniently [42], [49]. The frequency of the applied voltage is swept over the range 10 Hz – 100 kHz during impedance characterization. We opt to apply a voltage rather than apply a current because: i) voltage application is easier to manage as it produces a limited current at high impedances, and; ii) voltage application will be much easier to achieve with off-the-shelf electronics in future.

C. Sensor characterisation

To characterise temperature response, cured patches or samples of AAM are placed in an environmental chamber and cycled between 10 °C and 30 °C in steps of 5 °C. Samples are held at each temperature level for 2 hours to ensure thermal equilibrium of the concrete while the electrical impedance is measured.

For moisture / chloride characterisation, AAM sensor cells are immersed in deionized water / sodium chloride solutions for 24 hours to reach a high saturation. They are then gradually dried in stages via evaporation facilitated with a desiccator containing silica gel. The moisture levels are calculated at each stage based on the sample's mass using the gravimetric formula.

Damage to sensor cells can be deliberately induced by drilling holes into samples, or placing them under bend tests (if the concrete is reinforced). With some thought, the characterisations outlined above can also all be combined if the sensor response to multiple variables needs to be measured.

IV. Results and Discussion

A. Robotic deployment

Figure 4 shows examples of 3D printed and robotically spray-coated AAMs on concrete slabs. Extrusion is achieved with a screw cavity extruder fitted with a nozzle of size 18G (0.84 mm). The extruder is mobilsed via either a commercial 3D printer with an x-y gantry axis, or via a six-axis robot.

Typical variables of spray coating and 3D printing are: a spray pressure of 0.2 bar, a pump volume of 0.1 - 1 ml/min, a proximity from nozzle head to substrate of order 1 cm, and nozzle diameters of 0.5–0.9 mm.

These parameters are optimised for given patch geometry and material mix designs through trial and error. In general, increased robot head or gantry speeds require increased material flow to ensure constant patch thickness. 3D printed patches are typically deposited in one raster scan, while the spray coating process is made up of fast, sweeping motions and a large number of layers (10 or more). These approaches lead to a thorough coating of the substrate and allow small holes within the concrete surface to be filled with the AAM.

B. Temperature and moisture sensing

The overall response of the sensor for any general moisture and temperature combination is found by fitting temperature and moisture simultaneously using equation (4). The data points and fit are shown for a fly ash AAM in Figure 5, where parameters $G_1 = 0.8 \pm 0.4$, $G_2 = -0.012 \pm 0.003$ and $G_3 = 163 \pm 2$. In Figure 5 the 'dryness' of the sample is defined as the inverse of its moisture content, or $1/W$.

The behaviour shown is expected: both a reduction in moisture and temperature tend to cause an exponential increase in the measured electrical impedance. This means that the

Fig. 4. The (left) 3D printing and (right) robotic spray coating of AAM onto concrete slabs.

sensor does tend to show a more obvious impedance shift (and hence better measurement performance) at lower temperature and lower moisture contents, although it should be noted that electronics cannot be optimised for both high and low impedance measurements simultaneously (without switching at least), so this is more a case of matching interrogators to the environment faced. Overall, in our lab, we have found peak sensing performance at ambient temperatures and moisture levels (10–30 $°C$, 40–80 wt%).

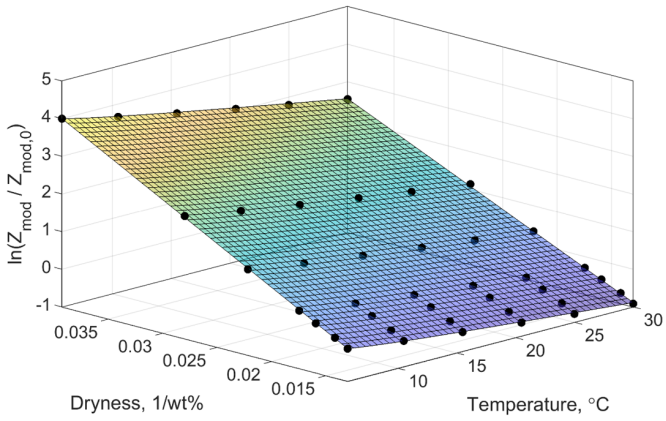

Fig. 5. The impedance response of an AAM sensor as a function of temperature and moisture (where dryness is the inverse of moisture).

C. Chloride sensing

Figure 6 shows some early results showing the shifts in fly ash AAM sensor impedance with sodium chloride contamination. As shown impedance decreases exponentially with increasing contamination, as expected. The results are promising and we have ongoing work in our group to fully characterise the shifts of the sensor in response to both chloride and moisture contamination.

D. Damage detection

Figure 7 shows early results indicating how a metakaolin AAM sensor responds to increasing levels of damage, where damage 3 >damage 2 >damage 1 >damage 0 (pristine sample). Damage was achieved in this case by drilling holes into the AAM sensor. Instead of monitoring impedance values, Figure 7 shows the current decay resulting from a square wave voltage input. This shows an alternative (perhaps more convenient) method of interrogating these sensors, as the current decay exponent and impedance of the sample are linked via changes in capacitance. Work is ongoing to assess how we can better quantify 'damage levels' and link these to impedance shifts.

V. Conclusions

This paper has outlined recent progress in our group's development of self-sensing repairs for concrete structures. The material's mechanical and adhesion properties are outlined in previous publications — this conference paper has focused

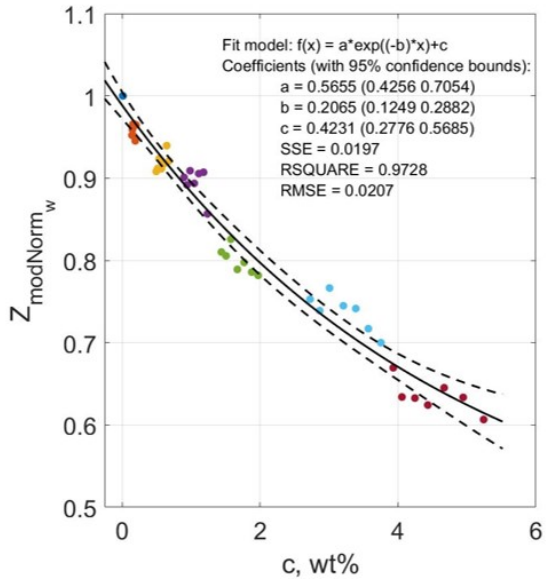

Fig. 6. Early results showing shifts in the impedance response of AAM sensors with increasing levels of chloride contamination.

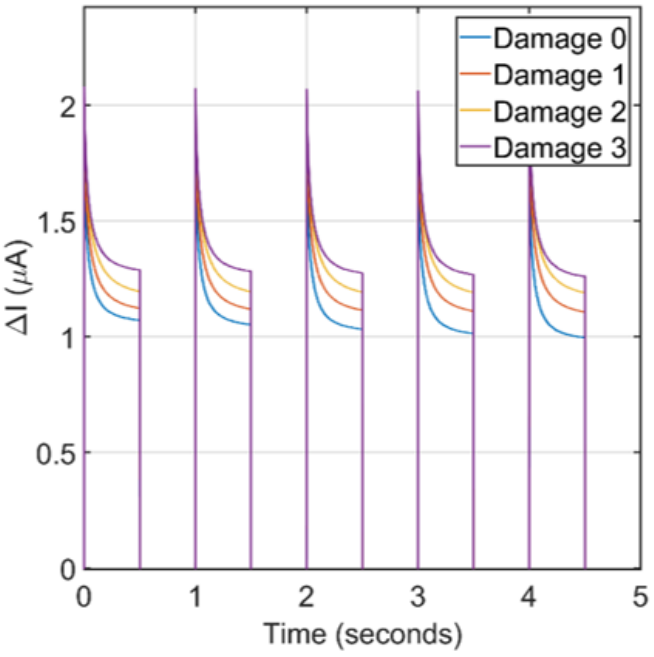

Fig. 7. Early results showing shifts in the impedance response of AAM sensors with increasing levels of damage.

on using the material to develop new moisture, chloride and damage sensors. Results in all cases are promising: the material shows exponential dependencies to increasing levels of internal water and ionic contamination. Work is ongoing to better characterise the sensor's response to damage both in the repair material itself, and the underlying concrete substrate.

References

[1] G. Koch, J. Varney, N. Thompson, O. Moghissi, M. Gould, and J. Payer, "NACE International Impact Report: International Measures of Prevention, Application, and Economics of Corrosion Technologies Study," Tech. Rep., 2016.

[2] US Department of Transportation, "Corrosion Cost and Preventive Strategies in the United States," Tech. Rep., 2002.

[3] US Dept Transportation, "2015 Status of the Nation's Highways, Bridges, and Transit: Conditions & Performance. Report to Congress," no. FHWA-PL-17-001. [Online]. Available: https://trid.trb.org/view/1445505

[4] S. Ion, "Nuclear energy: Current situation and prospects to 2020," vol. 365, no. 1853, pp. 935–944. [Online]. Available: http://rsta.royalsocietypublishing.org/content/365/1853/935

[5] OSTP, "Grand Challenges for Disaster Reduction and hazard-specific implementation Plans."

[6] European Commission (EC), "Research Theme Analysis Report: Transport Infrastructure."

[7] T. McDaniels, S. Chang, D. Cole, J. Mikawoz, and H. Longstaff, "Fostering resilience to extreme events within infrastructure systems: Characterizing decision contexts for mitigation and adaptation," vol. 18, no. 2, pp. 310–318. [Online]. Available: http://www.sciencedirect.com/science/article/pii/S0959378008000174

[8] J. L. Provis, "Geopolymers and other alkali activated materials: Why, how, and what?" *Materials and Structures*, vol. 47, no. 1, pp. 11–25, Jan. 2014.

[9] S. Hanjitsuwan, P. Chindaprasirt, and K. Pimraksa, "Electrical conductivity and dielectric property of fly ash geopolymer pastes," *International Journal of Minerals, Metallurgy, and Materials*, vol. 18, no. 1, pp. 94–99, 2011.

[10] X.-M. Cui, G.-J. Zheng, Y.-C. Han, F. Su, and J. Zhou, "A study on electrical conductivity of chemosynthetic Al2O3–2SiO2 geoplоymer materials," *Journal of Power Sources*, vol. 184, no. 2, pp. 652–656, 2008.

[11] M. Perry, M. Saafi, G. Fusiek, and P. Niewczas, "Hybrid optical-fibre/geopolymer sensors for structural health monitoring of concrete structures," *Smart Materials and Structures*, vol. 24, no. 4, p. 045011, 2015.

[12] ——, "Geopolymeric thermal conductivity sensors for surface-mounting onto concrete structures," in *9th International Concrete Conference*, Dundee, UK, 2016.

[13] M. Saafi, G. Piukovics, and J. Ye, "Hybrid graphene/geopolymeric cement as a superionic conductor for structural health monitoring applications," *Smart Materials and Structures*, vol. 25, no. 10, p. 105018, 2016.

[14] M. Saafi, L. Tang, J. Fung, M. Rahman, F. Sillars, J. Liggat, and X. Zhou, "Graphene fly ash geopolymeric composites as self-sensing structural materials," *Smart Materials and Structures*, vol. 23, no. 6, p. 065006, 2014.

[15] J. He, G. Zhang, S. Hou, and C. S. Cai, "Geopolymer-based smart adhesives for infrastructure health monitoring: Concept and feasibility," *Journal of Materials in Civil Engineering*, vol. 23, no. 2, pp. 100–109, 2010.

[16] L. Biondi, M. Perry, C. Vlachakis, Z. Wu, A. Hamilton, and J. McAlorum, "Ambient Cured Fly Ash Geopolymer Coatings for Concrete," *Materials*, vol. 12, no. 6, p. 923, 2019.

[17] F. Pacheco-Torgal, J. Castro-Gomes, and S. Jalali, "Alkali-activated binders: A review: Part 1." *Construction and Building Materials*, vol. 22, no. 7, pp. 1305–1314, Jul. 2008.

[18] T. L. Yeo, M. A. C. Cox, L. F. Boswell, T. Sun, and K. T. V. Grattan, "Optical fiber sensors for monitoring ingress of moisture in structural concrete," *Review of scientific instruments*, vol. 77, no. 5, p. 055108, 2006.

[19] T. L. Yeo, D. Eckstein, B. McKinley, L. F. Boswell, T. Sun, and K. T. V. Grattan, "Demonstration of a fibre-optic sensing technique for the measurement of moisture absorption in concrete," *Smart Materials and Structures*, vol. 15, no. 2, p. N40, 2006.

[20] Z. C. Grasley, D. A. Lange, M. D. D'Ambrosia, and S. Villalobos-Chapa, "Relative humidity in concrete," *Concrete international*, vol. 28, no. 10, pp. 51–57, 2006.

[21] R. M. Chacko, N. Banthia, and A. A. Mufti, "Carbon-fiber-reinforced cement-based sensors," *Canadian Journal of Civil Engineering*, vol. 34, no. 3, pp. 284–290, 2007.

[22] M. Saleem, M. Shameem, S. E. Hussain, and M. Maslehuddin, "Effect of moisture, chloride and sulphate contamination on the electrical resistivity of Portland cement concrete," *Construction and building materials*, vol. 10, no. 3, pp. 209–214, 1996.

[23] G. A. Woelfl and K. Lauer, "The electrical resistivity of concrete with emphasis on the use of electrical resistance for measuring moisture content," *Cement, concrete and Aggregates*, vol. 1, no. 2, pp. 64–67, 1979.

[24] G. E. Monfore, "A small probe-type gage for measuring relative humidity," Tech. Rep., 1963.

[25] P. Schie, L. W. Breot, and M. Raupach, "Investigations into the effect of coatings on water distribution in concrete using multi-ring electrodes," *Special Publication*, vol. 151, pp. 119–134, 1994.

[26] A. Schießl, W. J. Weiss, J. D. Shane, N. S. Berke, T. O. Mason, and S. P. Shah, "Assessing the moisture profile of drying concrete using impedance spectroscopy," *Concrete Science and Engineering(France)*, vol. 2, no. 6, pp. 106–116, 2000.

[27] I. Sánchez, C. Antón, G. De Vera, J. M. Ortega, and M. A. Climent, "Moisture distribution in partially saturated concrete studied by impedance spectroscopy," *Journal of Nondestructive Evaluation*, vol. 32, no. 4, pp. 362–371, 2013.

[28] K. Brantervik, A. Berg, G. A. Niklasson, B. Hedberg, and L.-O. Nilsson, "Percolation effects in the electrical conductivity of porous cement mortar," *EPL (Europhysics Letters)*, vol. 13, no. 6, p. 549, 1990.

[29] W. J. McCarter, G. Alaswad, and B. Suryanto, "Transient moisture profiles in cover-zone concrete during water absorption," *Cement and Concrete Research*, vol. 108, pp. 167–171, 2018.

[30] F. Rajabipour, J. Weiss, and D. M. Abraham, "Insitu electrical conductivity measurements to assess moisture and ionic transport in concrete (A discussion of critical features that influence the measurements)," in *Proceedings of the International RILEM Symposium on Concrete Science and Engineering: A Tribute to Arnon Bentur*, 2004.

[31] A. Q. Nguyen, G. Klysz, F. Deby, and J.-P. Balayssac, "Evaluation of water content gradient using a new configuration of linear array four-point probe for electrical resistivity measurement," *Cement and Concrete Composites*, vol. 83, pp. 308–322, 2017.

[32] L. J. Parrott, "Moisture profiles in drying concrete," *Advances in Cement Research*, vol. 1, no. 3, pp. 164–170, 1988.

[33] G. Hedenblad, *Moisture Permeability of Mature Concrete, Cement Mortar and Cement Paste*. Inst. of Technol., Division of Building Materials, 1993.

[34] L. Molina, *Measurement of High Humidity in Cementitious Material at an Early Age*. Swedish cement and concrete research institute, 1990.

[35] K. N. Mjörnell, "Moisture conditions in high performance concrete," *Chalmers University of Technology, Göteborg*, 1997.

[36] K. Norling Mjörnell, "Self-desiccation in concrete," *Report P-94*, vol. 2, pp. 21–28, 1994.

[37] A. Norris, M. Saafi, and P. Romine, "Temperature and moisture monitoring in concrete structures using embedded nanotechnology/microelectromechanical systems (MEMS) sensors," *Construction and building materials*, vol. 22, no. 2, pp. 111–120, 2008.

[38] Y. Yao and B. Glisic, "Sensing sheets: Optimal arrangement of dense array of sensors for an improved probability of damage detection," *Structural Health Monitoring*, vol. 14, no. 5, pp. 513–531, Sep. 2015.

[39] Z. Zhang, J. L. Provis, A. Reid, and H. Wang, "Fly ash-based geopolymers: The relationship between composition, pore structure and efflorescence," *Cement and Concrete Research*, vol. 64, pp. 30–41, 2014.

[40] P. Duxson, A. Fernández-Jiménez, J. L. Provis, G. C. Lukey, A. Palomo, and J. S. J. van Deventer, "Geopolymer technology: The current state of the art," *Journal of Materials Science*, vol. 42, no. 9, pp. 2917–2933, May 2007.

[41] K. Funke and R. D. Banhatti, "Ionic motion in materials with disordered structures," *Solid State Ionics*, vol. 177, no. 19-25, pp. 1551–1557, 2006.

[42] A. Lasia, "Electrochemical impedance spectroscopy and its applications," in *Modern Aspects of Electrochemistry*. Springer, 2002, pp. 143–248.

[43] N. Van Meurs, "Temperature dependence of the conductivity of electrolyte solutions," *Nature*, vol. 182, no. 4648, p. 1532, 1958.

[44] A. J. Durelli, "Experimental strain and stress analysis of solid propellant rocket motors," in *Mechanics and Chemistry of Solid Propellants*. Elsevier, pp. 381–442.

[45] Expedition Engineering, "Get It Right Initiative: Research Report Revision 3." [Online]. Available: http://getitright.uk.com/

[46] Y. Ding, A. Hellmann, and L. De Mello, "Factors driving memory fallibility: A conceptual framework for accounting and finance studies," *Journal of Behavioral and Experimental Finance*, vol. 14, pp. 14–22, Jun. 2017.

[47] W. E. Walker, P. Harremoës, J. Rotmans, J. P. van der Sluijs, M. B. A. van Asselt, P. Janssen, and M. P. K. von Krauss, "Defining Uncertainty: A Conceptual Basis for Uncertainty Management in Model-Based Decision Support," vol. 4, no. 1, pp. 5–17. [Online]. Available: https://doi.org/10.1076/iaij.4.1.5.16466

[48] F. L. Moon, A. E. Aktan, F. L. Moon, and A. E. Aktan, "Impacts of epistemic (bias) uncertainty on structural identification of constructed (civil) systems," *Shock Vibration Digest*, vol. 38, pp. 399–420, 2006.

[49] G. Instruments, "Basics of electrochemical impedance spectroscopy," *G. Instruments, Complex impedance in Corrosion*, pp. 1–30, 2007.